Water Dissociation on Graphene/Ir(111) Studied by Temperature-Dependent X-ray Photoelectron Spectroscopy

Juan Bernal Romero, Oscar Chavez, Carlos Rodriguez, Sebastian Gonzalez, Jael Fregoso, Vanessa Carbajal, Graciela Clavel, Owen Hudak, Jonathan Cheng, Joshua Tandoc, Jerome Brown, and Li Gao*

Department of Physics and Astronomy, California State University, Northridge, CA 91330, USA

Abstract

Water dissociation induced by graphene has been investigated by using temperature-dependent X-ray photoelectron spectroscopy (XPS) from 120 K to room temperature. Comparative studies on the interaction of water with the bare Ir(111) surface and submonolayer graphene/Ir(111) surface have observed graphene-induced spontaneous water dissociation above 160 K. The dominant role of graphene defects in the observed water dissociation has been corroborated by performing water exposure and XPS measurements of three different graphene/Ir(111) surfaces with different coverage and/or structural quality of the graphene layer. Our studies provide new relevant experimental insights into graphene-induced spontaneous water dissociation, which is valuable for understanding water-graphene interactions toward practical applications of graphene.

*Email: li.gao@csun.edu

Introduction

Graphene, a single atomic layer of carbon atoms bonded into a hexagonal honeycomb lattice, is the first discovered two-dimensional material with unique properties and various potential applications [1-3]. Understanding how graphene interacts with water is important for many practical applications such as water purification and desalination, energy storage and conversion, catalysis, coating, and various graphene-based devices working in ambient humidity [4-10]. Previous theoretical studies have suggested that the defects in graphene can catalyze the dissociation of water, which makes graphene a promising material for hydrogen production applications [11-13]. The dissociative adsorption of water on the graphene/Pt(111), graphene/Cu(111), and graphene/Ni(111) surfaces has been experimentally observed at room temperature by using high-resolution electron energy loss spectroscopy (HREELS) and X-ray photoelectron spectroscopy (XPS) [12-14]. The experimental studies on graphene-induced water dissociation have been primarily conducted at room temperature so far. The studies at 100 K did not observe water dissociation on the graphene/Pt(111) surface [14]. Therefore, it remains unknown what is the critical temperature for the occurrence of graphene-induced spontaneous water dissociation. Toward that end, temperature-dependent studies of the H_2O/graphene system below room temperature are needed but remain largely unexplored.

Here, we report on our studies of graphene-induced water dissociation using temperature-dependent XPS measurements from 120 K to room temperature. Our experiments were first performed on two different surfaces, bare Ir(111) surface and 0.78 monolayer (ML) graphene/Ir(111) surface, for comparative studies to identify the relevance of water dissociation to the graphene layer. The Ir(111) surface is chosen as the substrate for graphene because water does not dissociate on this surface [15], which is convenient for verifying the role of graphene

layer in water dissociation. We observed water dissociation on the graphene/Ir(111) surface but did not on the bare Ir(111) surface. The temperature-dependent XPS measurements indicate that the critical temperature for the occurrence of water dissociation on the graphene/Ir(111) surface is ~160 K. Further comparative studies of three different graphene/Ir(111) samples, with different coverage and/or structural quality, corroborate the dominant role of graphene defects in the observed water dissociation.

Materials and Methods

The sample preparations and scanning tunneling microscopy (STM) measurements were performed using a Unisoku ultra-high vacuum (UHV) low temperature STM system (USM1500S) with a base pressure lower than 2.0×10^{-10} Torr. The single crystal Ir(111) surface (Princeton Scientific) was cleaned by repeated cycles of Ar^+ ion sputtering (1.5 keV, 1.1×10^{-5} Torr, 40 min) at room temperature, annealing at 1100 ºC for 10 min, annealing in oxygen (2.5×10^{-7} Torr) at 1000 ºC for 20 min, flash annealing up to 1200 ºC, annealing in hydrogen (5.0×10^{-7} Torr) at 1000 ºC for 20 min, and flash annealing up to 1200 ºC. The cleanness of the prepared Ir(111) surface was checked using STM. The graphene/Ir(111) samples with numerous graphene domain boundaries were prepared by exposing the clean Ir(111) surface to ethylene (5×10^{-8} Torr) at 600 ºC for a selected time duration and subsequent annealing up to 900 ºC. The graphene/Ir(111) sample without graphene domain boundaries was prepared by exposing the clean Ir(111) surface to ethylene (2×10^{-8} Torr) at 900 ºC for a selected time duration and subsequent holding the sample at 900 ºC for additional 5 min. The coverage of graphene was controlled by ethylene exposure time and the number of growth cycles. The coverage and structural quality of graphene layer were checked using STM.

STM measurements were performed at 77 K with tungsten tips prepared by electrochemical etching and subsequent cleaning by e-beam heating in UHV. STM measurements were conducted in a constant-current mode. XPS measurements were performed using a Scienta Omicron XPS system with a Mg Kα X-ray source (1253.6 eV) and an Argus CU (R) hemispherical electron energy analyzer. The binding energy (BE) scale was calibrated using the clean Au ($4f_{7/2} = 84.0$ eV BE). The measurements were conducted with the X-ray photon beam impinging at angle of 30° with respect to the sample surface. The emitted photoelectrons were collected at an angle of 90° with respect to the sample surface. The O 1s XPS spectra were measured with a step size of 0.1 eV, a dwell time of 200 ms, and a pass energy of 20 eV. The O 1s XPS spectra shown here are the averaged signals of 10 scans for temperature dependent experiments and 100 scans for the experiments at ~180 K. Peak fitting was conducted using CasaXPS. XPS measurements were performed in the temperature range between 120 K and room temperature.

Water (Sigma Aldrich, deuterium depleted, ≤ 1 ppm (deuterium oxide)) was purified by freeze-pump-thaw cycles. The sample surfaces were exposed to water by introducing water vapor into the UHV chamber through a precision leak valve. The amount of water exposure was controlled by adjusting the exposure time while keeping the water gas pressure at 5.0×10^{-8} Torr. 1 Langmuir (L) exposure corresponds to 1.0×10^{-6} Torr $\cdot$ s. A UHV suitcase, with a base pressure of 5.0×10^{-10} Torr, was used for transferring samples between the UHV-STM system and the UHV-XPS system.

Results and Discussion

For the comparative studies, two samples were first prepared: the bare Ir(111) surface and 0.78 ML graphene/Ir(111) surface. Figure 1 (a) and (b) are the large scale STM images of these two

different surfaces. In Figure 1(c), the graphene edges are highlighted by green lines, the regions enclosed by green lines are Ir and the rest regions are graphene. The bare Ir regions are dispersedly distributed over the graphene/Ir surface, with a density of ~160 isolated bare Ir regions per square micrometer. The bright lines within the graphene layer on the STM images are domain boundaries. The number density of domains is around 1.0×10^3 per square micrometer. Figure 1(d) is an atomic-resolution STM image of the graphene domain boundaries. The three different domains D1, D2, and D3 have different Moiré patterns, and there exist defects at the boundaries between these domains.

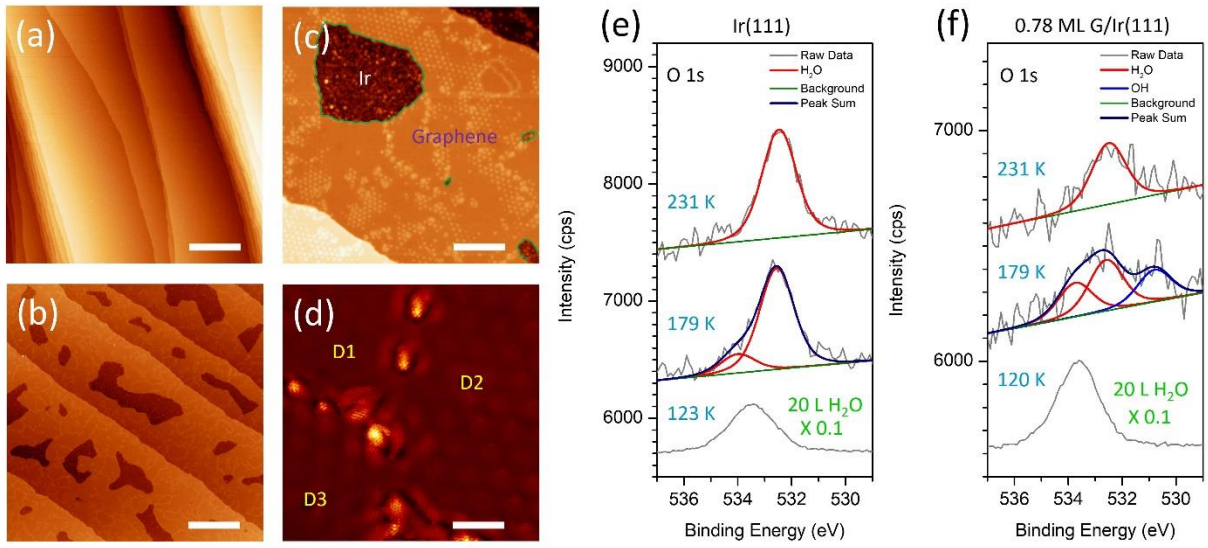

Figure 1: STM images of (a) the bare Ir(111) surface and (b-d) 0.78 ML graphene/Ir(111) surface. Scanning Parameters: (a-c) V_{bias} = 3 V, I_t = 10 pA; (d) V_{bias} = 10 mV, I_t = 9 nA. Scale Bars: (a-b) 80 nm; (c) 20 nm; (d) 4nm. In panel (c), graphene edges are highlighted by green lines, the regions enclosed by green lines are the Ir surface, and the rest regions are the graphene surface. Panel (d) is an atomic-resolution STM image of the graphene domain boundaries. D1,

D2, and D3 are three different graphene domains in this region. Temperature dependent XPS O 1s spectra on (e) the Ir(111) surface and (f) the 0.78 ML graphene/Ir(111) surface after they were exposed to 20 L H_2O at ~120 K and the temperature subsequently increased. The spectra are vertically shifted for clarity.

For temperature dependent XPS studies, the sample was first cooled down to ~120 K and then exposed to 20 L water. After that, the sample temperature was increased gradually from ~120 K up to room temperature with a step size of ~10 K. The XPS O 1s spectra were measured at each temperature step. The appearance of the OH component peak on the O 1s spectra is an indication for the occurrence of water dissociation on the surface. The O 1s electron binding energy is above 532 eV for H_2O molecules and 530-531 eV for OH groups, respectively [13, 16-20]. It is worth mentioning that the O 1s peak position for H_2O shifts toward higher BE for multilayer growth of H_2O [20].

Figure 1 (e) and (f) are the XPS O 1s spectra at three different temperatures during the temperature increase process for the bare Ir(111) sample and the 0.78 ML graphene/Ir(111) sample, respectively. At ~120 K, there is a huge H_2O peak but no visible OH peak for both samples. It is worth mentioning that water molecules adsorb molecularly and there is no water dissociation at 100 K on the graphene/Pt(111) surface [14]. At 179 K, the OH component peak (in blue) shows up for the graphene/Ir(111) sample but does not for the bare Ir(111) sample, which is a clear indication that graphene can catalyze water dissociation at this temperature. At 231 K, there are only H_2O peaks for both samples and the OH component peak is no longer visible for the graphene/Ir(111) sample.

Figure 2(a) shows the area intensity of H_2O component peaks on the O 1s spectra as a function of temperature. The main desorption process was observed from ~150 K to ~170 K for

the Ir(111) surface and from ~140 K to ~160 K for the graphene/Ir(111) surface. The difference in desorption temperature between the two samples is induced by the graphene layer. Water molecules desorb from the graphene/Ir(111) surface more easily than from the Ir(111) surface. For the temperature range from 200 K to room temperature, the amount ratio of H_2O on the graphene/Ir(111) sample to H_2O on the Ir(111) sample is 0.24 ± 0.03. For the 0.78 ML graphene/Ir(111) sample, ~22% of the sample surface area is Ir. These results suggest that, above 200 K, the remaining H_2O molecules on the submonolayer graphene/Ir(111) sample are primarily in the Ir regions; however, we cannot exclude the possibility that there are some water molecules at the graphene/Ir(111) interface [13]. It is worth mentioning that the desorption of water molecules from the graphene/Pt(111) surface occurs at 140 K [14], similar to the desorption temperature we have observed for the graphene/Ir(111) surface.

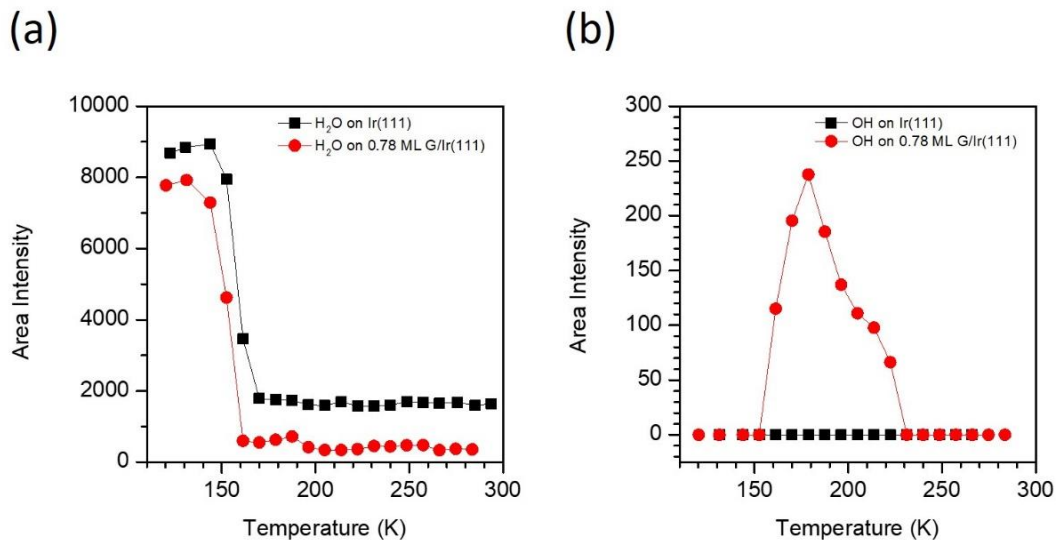

Figure 2: Temperature dependent area intensity of H_2O and OH component peaks on the Ir(111) sample and the 0.78 ML graphene/Ir(111) sample after they were exposed to 20 L H_2O at ~120 K and the temperature subsequently increased up to room temperature gradually.

Figure 2(b) shows the area intensity of the OH component peak of the O 1s spectra as a function of temperature. On the bare Ir(111) sample, no OH group was detected by XPS for the temperature range from 120 K to room temperature. For the graphene/Ir(111) surface, the OH group started appearing on the surface at ~160 K, reached its maximum amount at ~180 K, and then decreased down to zero at ~230 K. The appearance of OH groups on the surface indicates the occurrence of water dissociation on the graphene/Ir(111) surface. The comparison between these two samples unambiguously shows that graphene can induce water dissociation above ~160 K. When the temperature increases from 160 K to 180 K, the water dissociation is enhanced with increasing temperature, which leads to the amount increase of OH groups on the surface. The decrease of OH amount with increasing temperature above 180 K is most likely due to the enhanced desorption of OH groups from the surface and/or its recombination with atomic H.

The dissociation of water produces OH group and atomic H on the surface. Atomic H is stable on the graphene surface even at room temperature [21-22]. Hydrogenation of the graphene/metal surfaces after water dosing at room temperature has been observed for graphene/Pt(111) [14], graphene/Cu(111) [12], graphene/Ru(0001) [23] and graphene/Ni(111) [13]. So the generated H atoms largely stay on the graphene surface during our temperature dependent experiments up to room temperature. In a previous HREELS study of water adsorption on the graphene/Pt(111) surface at room temperature, the vibrational modes of OH groups are absent, which indicates that the adsorption energy of OH groups is positive in the presence of co-adsorbed H atoms on the graphene surface and the OH groups are not stable at room temperature [14]. That may partly explain our observation that the amount of OH groups on the graphene/Ir(111) surface decreases from its maximum down to zero when the temperature

increases from ~180 K to ~230 K. In the initial stage of water dissociation (~160 K), the OH groups can largely stay on the surface as the amount of atomic H on the surface is very low. As water dissociation continues, more and more H atoms are generated on the surface, and it gets harder and harder for OH groups to stay on the surface. At a certain point, the OH groups start desorbing from the surface with increasing temperature and/or recombination with atomic H due to the rich presence of atomic H on the surface. That is a possible reason why, during our temperature dependent studies, the OH groups generated by water dissociation were detected by XPS only within a certain temperature range.

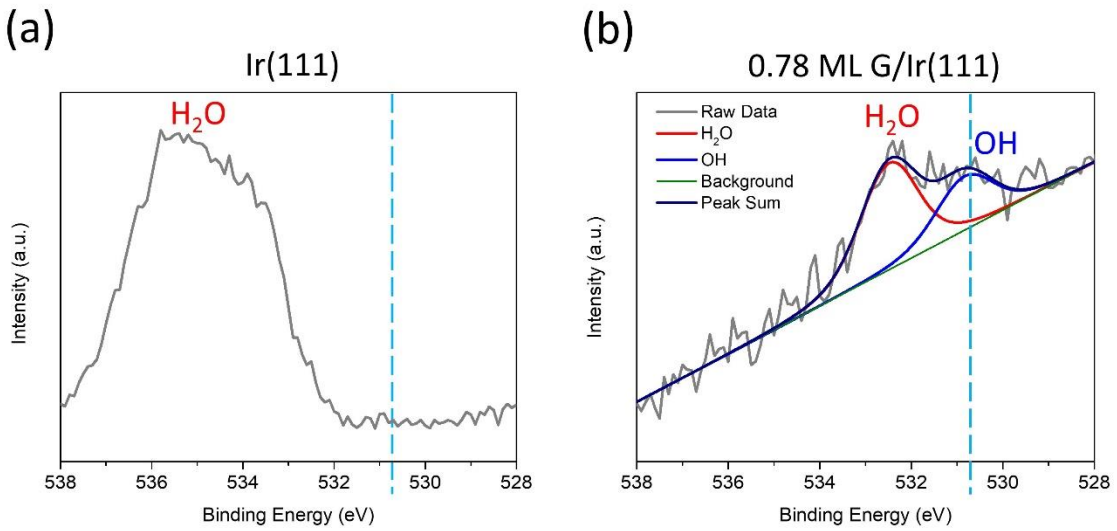

Figure 3: XPS O 1s spectra of the Ir(111) sample and the 0.78 ML Graphene/Ir(111) sample after they were exposed to 100 L H_2O at ~180 K. The dashed line indicates the binding energy position for the OH component peak.

As shown in Figure 2(b), the detected OH amount on the graphene/Ir(111) surface reaches its maximum at ~180 K. The signal-to-noise ratio for the OH component peak shown in Figure

1(f) is not very high because the starting dosage at ~120 K was only 20 L and the acquisition time for each O 1s spectrum was limited during the temperature-dependent experiments. To improve the signal-to-noise ratio and further verify the difference in O 1s spectra between the bare Ir(111) surface and the graphene/Ir(111) surface, additional experiments were performed as shown in Figure 3. The samples were first cooled down to ~180 K and then exposed to 100 L water vapor. After that, the O 1s spectra were measured with a much longer acquisition time while the temperature was maintained at ~180 K. Figure 3 clearly shows that the OH component peak (in blue) appeared for the 0.78 ML graphene/Ir(111) surface but did not for the bare Ir(111) surface.

As shown in Figure 1(b-d), there are many graphene edges and domain boundaries on the 0.78 ML graphene/Ir(111) surface. As water molecules have a high dissociation barrier, it has been suggested that water dissociation should occur at defects in graphene [11-13]. In order to experimentally verify the dependence of water dissociation on graphene edges and domain boundaries, we have prepared two additional graphene/Ir(111) samples for comparative studies: 1 ML graphene with numerous domain boundaries and 1 ML graphene without domain boundaries. Their STM images are shown in Figure 4 (a-b) and (c-d), respectively. On the sample surface shown in Figure 4(a-b), there exist numerous different graphene domains with different Moiré patterns. In contrast, on the sample surface shown in Figure 4(c-d), there exists only a single graphene domain. The XPS O 1s spectra were measured on these two samples after they had been exposed to 100 L water at ~180 K. The OH group was detected on the 1 ML graphene/Ir(111) sample with numerous domain boundaries but not on the 1 ML graphene/Ir(111) sample without domain boundaries, as shown in Figure 4 (e) and (f), respectively. Figure 4(g) shows the XPS peak area intensities of H_2O and OH for water dosing experiments on the above-

mentioned three different graphene/Ir samples at ~180 K. The amount of adsorbed water molecules is much larger on the 0.78 ML graphene/Ir surface than on the other two 1 ML graphene/Ir surfaces, which indicates that the sticking coefficient of water molecules on the Ir surface is much larger than on the graphene/Ir surface. The OH groups were detected on the two samples with defects: 0.78 ML graphene/Ir sample with graphene edges and domain boundaries and 1 ML graphene/Ir sample with domain boundaries. There is no detectable amount of OH groups on the 1 ML graphene/Ir sample without domain boundaries. The comparison between these three samples clearly indicates that the defects in graphene increase the chemical reactivity of graphene and play a dominant role in the observed water dissociation.

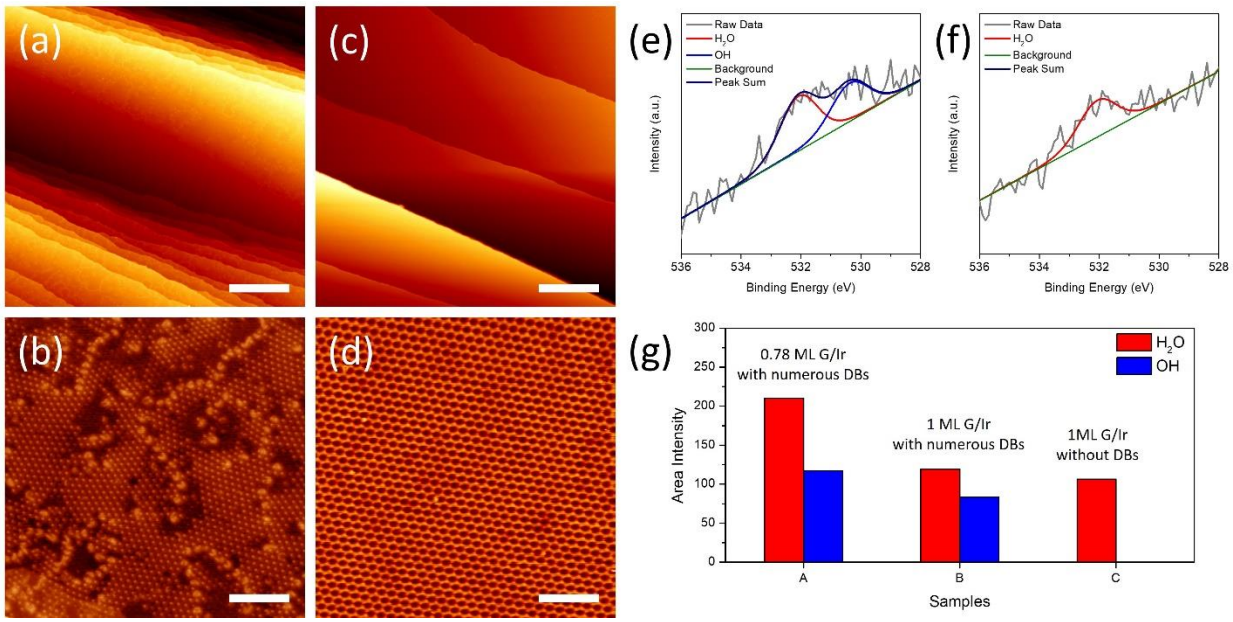

Figure 4: (a-b) STM images of 1 ML graphene/Ir with numerous domain boundaries. (c-d) STM images of 1 ML graphene/Ir without domain boundaries. Scanning Parameters: (a-c) V_{bias} = 3 V, I_t = 10 pA; (d) V_{bias} = 2 V, I_t = 10 pA. Scale Bars: (a) 80 nm; (b) 20 nm; (c) 60 nm; (d) 20 nm. (e) XPS O 1s spectra of the surface shown in (a-b) after it was exposed to 100 L H_2O at

~180 K. (f) XPS O 1s spectra of the surface shown in (c-d) after it was exposed to 100 L H_2O at ~180 K. (g) XPS peak area intensities of H_2O and OH on three different graphene/Ir samples after they were exposed to 100 L H_2O at ~180 K.

Density functional theory (DFT) calculations have been conducted to explore the mechanisms for water dissociation induced by graphene edges and domain boundaries on the graphene/metal surfaces [12-13]. He *et al*. found that the energy barrier for water dissociation at the graphene edge on the graphene/Cu(111) surface is as low as 0.35 eV, which is significantly lower than the energy barrier 3.64 eV on bare pristine graphene [12, 24]. The graphene edge is saturated by H and decoupled from the Cu substrate after water dissociation at the edge, which allows water to migrate into the graphene/Cu interface and decompose there. The promotion of water dissociation at the interface has been ascribed to the limited space that enhances the O-H bond stretch and the charge transfer between Cu, H_2O, and graphene [12]. DFT studies by Politano *et al*. suggest that water can penetrate into the graphene/Ni(111) interface through graphene domain boundaries and decomposes at the interface [13]. The defects at the graphene domain boundaries increase the chemical reactivity of graphene and promote the dissociation of water. The mechanisms described above for graphene/Cu(111) and graphene/Ni(111) surfaces possibly also apply to the graphene/Ir(111) surface, which needs to be verified by future detailed theoretical studies.

Conclusion

In summary, we have observed the graphene-induced spontaneous water dissociation by performing temperature dependent XPS studies of several comparative samples including the bare Ir(111) surface and three graphene/Ir(111) surfaces. Our results indicate that the critical

temperature for the occurrence of water dissociation on the graphene/Ir(111) surface is ~160 K. Comparative studies of three different graphene/Ir samples indicate the dominant role of graphene defects in the observed water dissociation. Our findings provide new relevant experimental insights into the graphene-induced spontaneous water dissociation and are valuable for understanding the water-graphene interactions toward relevant practical applications.

Data Availability

The data for this article are available from the corresponding author upon reasonable request.

Conflict of Interest

On behalf of all authors, the corresponding author states that there is no conflict of interest.

References:

1. K.S. Novoselov, A.K. Geim, S.V. Morozov, D. Jiang, Y. Zhang, S.V. Dubonos, I.V. Grigorieva, A.A. Firsov, Electric field effect in atomically thin carbon films. Science **306,** 666-669 (2004).
https://doi.org/10.1126/science.1102896

2. S.K. Tiwari, S. Sahoo, N. Wang, A. Huczko, Graphene research and their outputs: Status and prospect. J. Sci: Adv. Mater.Devices **5**(1), 10-29 (2020).
https://doi.org/10.1016/j.jsamd.2020.01.006

3. A.H. Castro Neto, F. Guinea, N.M.R. Peres, K.S. Novoselov, A.K. Geim, The electronic properties of graphene. Rev. Mod. Phys. **81**(1), 109-162 (2009).
https://doi.org/10.1103/RevModPhys.81.109

4. C. Melios, C.E. Giusca, V. Panchal, O. Kazakova, Water on graphene: Review of recent progress. 2D Mater. **5**(2), 022001 (2018).
https://doi.org/10.1088/2053-1583/aa9ea9

5. S. Homaeigohar, M. Elbahri, Graphene membranes for water desalination. NPG Asia Mater. **9**, e427 (2017).
https://doi.org/10.1038/am.2017.135

6. M. Pandey, K. Deshmukh, A. Raman, A. Asok, S. Appukuttan, G.R. Suman, Prospects of MXene and graphene for energy storage and conversion. Renew. Sustain. Energy Rev. **189**, 114030 (2024).
https://doi.org/10.1016/j.rser.2023.114030

7. P.Z. Sun, W.Q. Xiong, A. Bera, I. Timokhin, Z.F. Wu, A. Mishchenko, M.C. Sellers, B.L. Liu, H.M. Cheng, E. Janzen, J.H. Edgar, I.V. Grigorieva, S.J. Yuan, A.K. Geim, Unexpected catalytic activity of nanorippled graphene. Proc. Natl. Acad. Sci. **120**(12), e2300481120 (2023).
https://doi.org/10.1073/pnas.2300481120

8. J. Ruhkopf, U. Plachetka, M. Moeller, O. Pasdag, I. Radev, V. Peinecke, M. Hepp, C. Wiktor, M.R. Lohe, X. Feng, B. Butz, M.C. Lemme, Graphene coating of nafion membranes for enhanced fuel cell performance. ACS Appl. Eng. Mater. **1**(3), 947-954 (2023).
https://doi.org/10.1021/acsaenm.2c00234

9. J. Cai, E. Griffin, V.H. Guarochico-Moreira, D. Barry, B. Xin, M. Yagmurcukardes, S. Zhang, A.K. Geim, F.M. Peeters, M. Lozada-Hidalgo, Wien effect in interfacial water dissociation through proton-permeable graphene electrodes. Nat. Commun. **13**(1), 5776 (2022). https://doi.org/10.1038/s41467-022-33451-1

10. M. Sacchi, A. Tamtögl, Water adsorption and dynamics on graphene and other 2D materials: Computational and experimental advances. Adv. Phys.: X **8**(1), 2134051 (2023). https://doi.org/10.1080/23746149.2022.2134051

11. M.K. Kostov, E.E. Santiso, A.M. George, K.E. Gubbins, M.B. Nardelli, Dissociation of water on defective carbon substrates. Phys. Rev. Lett. **95**(13), 136105 (2005). https://doi.org/10.1103/PhysRevLett.95.136105

12. G. He, Q. Wang, H.K. Yu, D. Farías, Y. Liu, A. Politano, Water-induced hydrogenation of graphene/metal interfaces at room temperature: Insights on water intercalation and identification of sites for water splitting. Nano Res. **12**(12), 3101-3108 (2019). https://doi.org/10.1007/s12274-019-2561-y

13. A. Politano, M. Cattelan, D.W. Boukhvalov, D. Campi, A. Cupolillo, S. Agnoli, N.G. Apostol, P. Lacovig, S. Lizzit, D. Farías, G. Chiarello, G. Granozzi, R. Larciprete, Unveiling the mechanisms leading to H_2 production promoted by water decomposition on epitaxial graphene at room temperature. ACS Nano **10**(4), 4543-4549 (2016). https://doi.org/10.1021/acsnano.6b00554

14. A. Politano, A.R. Marino, V. Formoso, G. Chiarello, Water adsorption on graphene/Pt(111) at room temperature: A vibrational investigation. AIP Adv. **1**(4), 042130 (2011). https://doi.org/10.1063/1.3660325

15. A. Shavorskiy, M.J. Gladys, G. Held, Chemical composition and reactivity of water on hexagonal Pt-group metal surfaces. Phys. Chem. Chem. Phys. **10**(40), 6150-6159 (2008). https://doi.org/10.1039/B808235A

16. S. Yamamoto, K. Andersson, H. Bluhm, G. Ketteler, D.E. Starr, T. Schiros, H. Ogasawara, L.G.M. Pettersson, M. Salmeron, A. Nilsson, Hydroxyl-induced wetting of metals by water at near-ambient conditions. J. Phys. Chem. C **111**(22), 7848-7850 (2007). https://doi.org/10.1021/jp0731654

17. K. Andersson, A. Gómez, C. Glover, D. Nordlund, H. Öström, T. Schiros, O. Takahashi, H. Ogasawara, L.G.M. Pettersson, A. Nilsson, Molecularly intact and dissociative adsorption of water on clean Cu(110): A comparison with the water/Ru(001) system. Surf. Sci. **585**(3), L183-L189 (2005).
https://doi.org/10.1016/j.susc.2005.04.024

18. S. Yamamoto, H. Bluhm, K. Andersson, G. Ketteler, H. Ogasawara, M. Salmeron, A. Nilsson, In situ x-ray photoelectron spectroscopy studies of water on metals and oxides at ambient conditions. J. Phys.: Condens. Matter **20**(18), 184025 (2008).
https://doi.org/10.1088/0953-8984/20/18/184025

19. D.V. Sivkov, O.V. Petrova, S.V. Nekipelov, A.S. Vinogradov, R.N. Skandakov, K.A. Bakina, S.I. Isaenko, A.M. Ob'edkov, B.S. Kaverin, I.V. Vilkov, V.N. Sivkov, Quantitative characterization of oxygen-containing groups on the surface of carbon materials: XPS and NEXAFS study Appl. Sci. **12**(15), 7744 (2022).
https://doi.org/10.3390/app12157744

20. H.S. Casalongue, S. Kaya, V. Viswanathan, D.J. Miller, D. Friebel, H.A. Hansen, J.K. Nørskov, A. Nilsson, H. Ogasawara, Direct observation of the oxygenated species during oxygen reduction on a platinum fuel cell cathode. Nat. Commun. **4**(1), 2817 (2013).
https://doi.org/10.1038/ncomms3817

21. P. Sessi, J.R. Guest, M. Bode, N.P. Guisinger, Patterning graphene at the nanometer scale via hydrogen desorption. Nano Lett. **9**(12), 4343-4347 (2009).
https://doi.org/10.1021/nl902605t

22. L. Gao, P.P. Pal, T. Seideman, N.P. Guisinger, J.R. Guest, Current-driven hydrogen desorption from graphene: Experiment and theory. J. Phys. Chem. Lett. **7**(3), 486-494 (2016).
https://doi.org/10.1021/acs.jpclett.5b02471

23. A. Politano, G. Chiarello, Periodically rippled graphene on Ru(0001): A template for site-selective adsorption of hydrogen dimers via water splitting and hydrogen-spillover at room temperature. Carbon **61,** 412-417 (2013).
https://doi.org/10.1016/j.carbon.2013.05.025

24. Z. Xu, Z. Ao, D. Chu, A. Younis, C.M. Li, S, Li, Reversible hydrophobic to hydrophilic transition in graphene via water splitting induced by UV irradiation. Sci. Rep. **4**, 6450 (2014).
https://doi.org/10.1038/srep06450

Author Contributions

The experiments were performed by all authors. JBR and LG analyzed the data. LG supervised the project and wrote the manuscript with input from all authors.

Funding

We gratefully acknowledge the financial support from the National Science Foundation (NSF) (Grants No. DMR-1809805 and No. DMR-1828019) and California State University Northridge. The XPS measurements were performed on an instrument acquired with financial support from the U.S. Army Research Office (Contract #: W911NF-17-1-0459).